Journal of Catalysis **195,** 88–95 (2000)
doi:10.1006/jcat.2000.2967, available online at http://www.idealibrary.com on IDEAL®

Palladium, Palladium–Tin, and Palladium–Silver Catalysts in the Selective Hydrogenation of Hexadienes: TPR, Mössbauer, and Infrared Studies of Adsorbed CO

Emerson Andrade Sales,*,‡,[1] Jose Jove,† Mario de Jesus Mendes,‡ and François Bozon-Verduraz*,[2]

*Laboratoire de Chimie des Matériaux Divisés et Catalyse, Université Paris, 7, case 7090, 2, place Jussieu, 75251 Paris Cedex 05, France; †Laboratoire de Magnetisme et d'Optique, URA D1531, Université de Versailles, Bâtiment Fermat, 45 avenue des Etats Unis, 78035 Versailles Cedex, France; ‡Faculdade de Engenharia Química, Unicamp, C.P. 6066, 13083-970, Campinas São Paulo, Brazil

Received March 5, 2000; revised June 13, 2000; accepted June 13, 2000

Alumina-supported Pd–Sn catalysts prepared by successive impregnation of the precursors, calcination, and reduction contain SnO_2 and $SnAl_2O_5$, Pd–Sn solid solutions, and intermetallic phases Pd_2Sn and Pd_3Sn. The formation of Pd_3Sn is favored not only by lowering the Sn/Pd ratio but also by introducing tin through ethanolic impregnation. The dilution of surface Pd atoms is confirmed by infrared spectroscopy of adsorbed CO: when the Sn/Pd ratio increases, the linear/bridged intensity ratio increases and the dipole–dipole interactions decrease. TPR experiments show the influence of the support acidity and of the preparation procedure on the reducibility of the various Pd–Sn and Pd–Ag species; in the case of Pd–Ag catalysts, the presence of silver *postpones* **the reduction of PdO in calcined samples.**

Key Words: **Pd catalysts; Pd–Sn catalysts; Pd–Ag catalysts; Mössbauer spectroscopy; CO adsorption; FTIR spectroscopy; Pd–Sn compounds.**

1. INTRODUCTION

In opposition to the selective hydrogenation of buta-1,3-diene (1, 2), the hydrogenation of heavier dienes has attracted little attention, although some important industrial applications concern C_{6+} unsaturated hydrocarbons, e.g., the selective hydrogenation of C_{11}–C_{13} alkadienes present as impurities in alkenes employed in the production of linear alkylbenzenes used as surfactants. The hydrogenation of hexa-1,3-diene and hexa-1,5-diene in the liquid phase may be used as a *model reaction* for the hydrogenation of C_{11}–C_{13} alkadienes; this reaction has already been investigated on *monometallic* palladium catalysts (3) but, to our knowledge, not on *bimetallic* systems, except for a study from our laboratory devoted to Pd and Pd–Ag catalysts prepared by the polyol process (4). The general aim of our studies is to examine the influence of the addition of a second metal on activity and selectivity of Pd/alumina catalysts; the effects of tin and silver were investigated first; in a previous paper (5), the preparation of Pd–Sn and Pd–Ag alumina-supported catalysts was described, in addition to the characterization of the solutions used for impregnation and of the solids obtained at the different stages of preparation. The aim of the present work is to achieve the characterization by Mössbauer studies, temperature-programmed reduction (TPR), and surface investigations by IR spectroscopy of adsorbed CO. The catalytic performances are detailed elsewhere (6).

2. EXPERIMENTAL

2.1. Materials

The catalysts preparation was described previously (5); shortly, it consists of (i) simple or successive diffusional impregnation of the precursors: $PdCl_2$, $SnCl_2$ in aqueous hydrochloric solution, and $Ag(NH_3)^{2+}$; (ii) drying at 383 K; (iii) calcination at 773 K; and (iv) reduction under flowing hydrogen at 773 K. Both alumina supports were supplied by Alcoa: (i) Support A1: surface area 63 m^2/g; $\alpha+\gamma$ phases; pore volume, 0.9 cm^3/g; zero point charge (ZPC) = 8.4. (ii) Support A2: surface area 62 m^2/g; γ phase; pore volume, 0.6 cm^3/g; ZPC = 5.9. Table 1 summarizes the catalyst notation and metal loading. In one Pd–Sn sample ($Pd_{4.9}Sn_{5.0}Et/A1$), tin was introduced from an ethanolic solution of $SnCl_2$.

2.2. Methods

The Fourier transform infrared (FTIR) spectra were recorded at room temperature (r.t.) on a Perkin-Elmer 1750 spectrometer, at a resolution of 2 cm^{-1} using around 100 scans. Sample disks (diameter, 18 mm; mass, 35 mg; transmittance, around 30%) of reduced samples were put

[1] Present address: Instituto de Química, Universidade Federal da Bahia, Campus Universitário de Ondina, 40170-290 Salvador, Bahia, Brazil. E-mail: eas@ufba.br.

[2] To whom correspondence should be addressed. Fax: 33-1-44276137. E-mail: bozonver@ccr.jussieu.fr.

0021-9517/00 $35.00

TABLE 1

Catalysts Identification and Metal Loading (wt%)

Identification	%Pd	%Sn	%Ag	Sn/Pd or Ag/Pd atomic ratio
01. $Pd_{5.0}$/A1	5.05	—	—	—
02. $Pd_{5.1}Sn_{3.8}$/A1	5.14	3.79	—	0.66
03. $Pd_{4.9}Sn_{5.0}$Et/A1	4.89	4.96	—	0.91
04. $Pd_{5.2}Sn_{0.8}$/A1	5.17	0.77	—	0.13
05. $Pd_{4.9}Ag_{5.1}$/A1	4.93	—	5.13	1.03
06. $Sn_{4.9}$/A1	—	4.93	—	—
07. $Pd_{4.6}$/A2	4.55	—	—	—
08. $Pd_{4.1}Sn_{4.5}$/A2	4.12	4.50	—	0.98
09. $Pd_{3.8}Ag_{5.2}$/A2	3.77	—	5.24	1.37

into an infrared cell equipped with CaF_2 windows, designed to treat the samples in a controlled atmosphere. They were submitted to the following pretreatment: (i) outgassing at r.t. for 3 h; (ii) reduction under flowing hydrogen at a programmed temperature (5 K/min) from 293 to 573 K, plus 30 min at 573 K; (iii) outgassing (10^{-2} mbar) overnight at 573 K, before introduction of CO at r.t. and IR measurements. The spectra presented here were obtained after subtracting the gas phase and solid contributions. Temperature-programmed reduction (TPR) of calcined samples were carried out on equipment similar to that described in (7), but the whole apparatus was designed around a six-way valve, using mainly 1/16″ tubing, to minimize the dead volumes. The procedure included stabilization of both N_2 and H_2 (2.0 mol% in N_2) baselines, purge of the catalyst with N_2 (catalyst mass, 100 mg; temperature, 253 K), exposure to the reducing mixture, warming to r.t. (295 K), and heating up to 773 K (heating rate, 10 K/min).

Mössbauer spectra of both calcined and reduced supported Pd–Sn samples, of Sn/Al_2O_3, and of pure SnO_2 samples were obtained at room temperature using a constant acceleration spectrometer with a 10mCi $Ca^{119}SnO_3$ source. The Mössbauer parameters were determined by Lorentzian lines computer fitted by the least squares method. The isomer shift parameters were reported with respect to SnO_2.

X-ray photoelectron spectroscopy (XPS) was performed on an SSX-100 spectrometer (Surface Science Laboratory); the Al 2*p* peak (74.6 eV) was used as a reference; experimental details are available in Ref. (4).

3. RESULTS AND DISCUSSION

3.1. FTIR Spectra of Adsorbed CO

Two kinds of CO adsorption experiments were performed: under *rising CO pressure*, to follow the formation of the absorption bands, and under *decreasing CO pressure*, to compare the adsorption strength of the various species involved.

On the monometallic catalyst $Pd_{5.0}$/A1 (Fig. 1a), four bands were observed, at around 2160 cm^{-1} (A), 2100 cm^{-1} (B), 1995 cm^{-1} (C), and 1970 cm^{-1} (D), with a shoulder (E) at about 1930 cm^{-1}, A and B being much less intense than C, D, and E.

The weak band A is attributed to the interaction of CO (a "soft" base) with residual surface Pd^{2+} ions (8, 9). It is relevant to note that CO interaction with the "hard" ions Al^{3+} present on the dehydrated alumina surface generates weak bands at higher wavenumbers (2195–2245 cm^{-1}) (9, 10), not detected in the present work. These residual Pd^{2+} ions should be stabilized by neighboring chloride ions, present in all prepared catalysts (Cl/Pd = 1.34 in $Pd_{5.0}$/A1 after calcination) (5), and not removed by the reduction procedure used (773 K for 10 min under 5% H_2/He).

The band B is ascribed to linear CO species adsorbed on metallic Pd. This band may contain several components

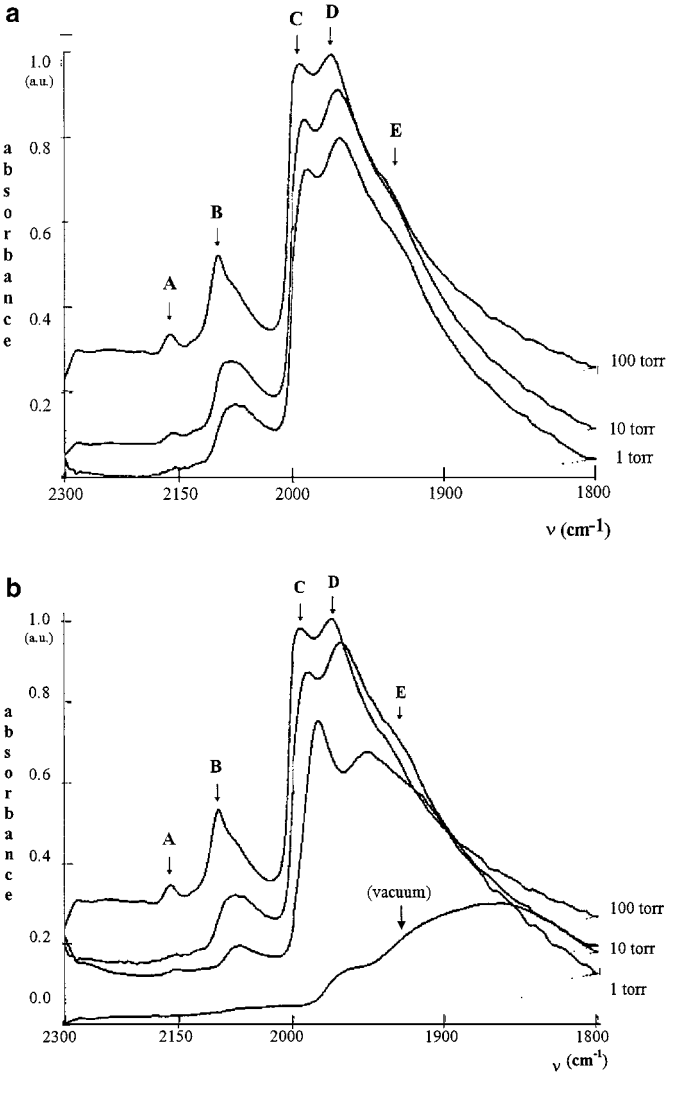

FIG. 1. Sample $Pd_{5.0}$/A1. IR spectrum of CO adsorbed under (a) *increasing* pressure; (b) *decreasing* pressure.

corresponding to CO interaction with Pd atoms located on different Pd crystal planes (111, 100, 110), with different coordination numbers (9, 8, and 7 respectively) (8, 11). The C, D, and E bands are ascribed to CO bridged species located on different Pd crystal planes and/or submitted to dipole–dipole coupling of different intensities. Experiments performed on decreasing CO pressure (Fig. 1b) allow a better understanding of the structure of the species involved: when the CO pressure is lowered from 100 to 1 Torr (1 Torr = 133.3 N m^{-2}), A is removed first as CO is weakly bonded to Pd^{2+}; B is shifted toward lower wavenumbers with a marked intensity decrease as the stability is smaller for Pd sites of higher coordination and also as the dipole–dipole coupling is suppressed. C, D, and E are also shifted toward lower wavenumbers but without appreciable drop of intensity. These variations suggest that three types of bridged species are involved (8, 9, 12): (i) compressed bridged CO species in direct interaction with linear CO, called B_2L species; (ii) *compressed* bridged species (B_2), i.e., bridged carbonyl groups in direct interaction with each other; (iii) *isolated* bridged CO:

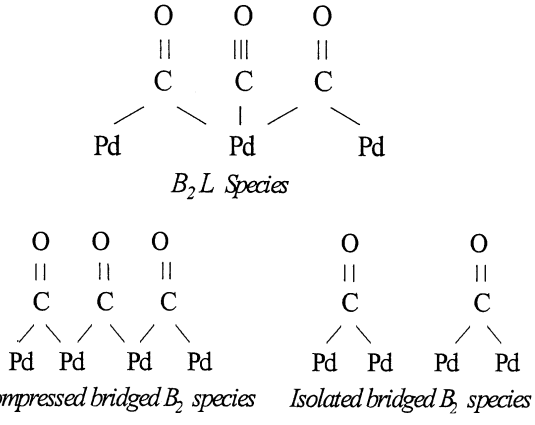

Removing linear species diminishes the coupling between vibrators and, hence, the frequency. Finally, the E band, which remains on the surface even after outgassing at 373 K for 30 min, is ascribed to B_2 species interacting with low coordination planes or to a tricoordinated $Pd_3(CO)$ entity (B_3).

For catalyst $Pd_{5.2}Sn_{0.8}$/A1 (Sn/Pd atomic ratio = 0.13), the formation of both linear and bridged carbonyls is also observed but with a greater linear/bridged intensity ratio upon either increasing (Fig. 2a) or decreasing CO pressure (Fig. 2b); this is explained by a dilution of Pd atoms by Sn atoms, which lowers the probability of formation of bridged species. In addition, the surface species seem to be less firmly attached than on the monometallic catalyst $Pd_{5.0}$/A1; i.e., the presence of tin appears to weaken the CO adsorption strength; this is not unexpected as linear entities are less firmly bonded than bridged ones and it is not necessary to involve an electronic effect of tin on palladium. It is also relevant to note that, for linear species,

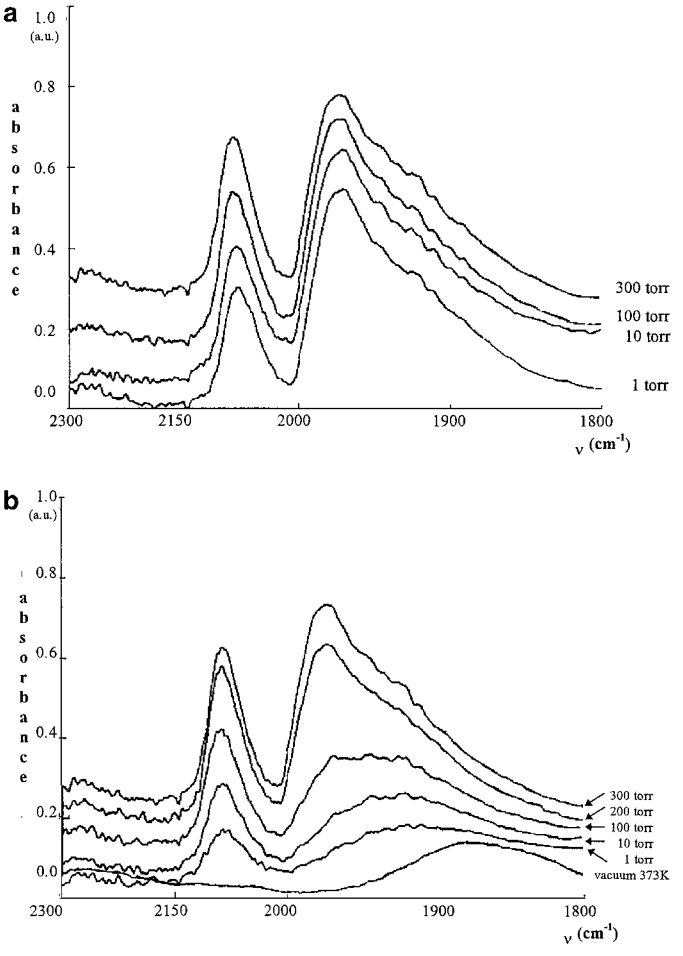

FIG. 2. Sample $Pd_{5.2}Sn_{0.8}$/A1. IR spectrum of CO adsorbed under (a) *increasing* pressure; (b) *decreasing* pressure.

the wavenumber shift upon decreasing CO pressure is very small, which confirms that dipole–dipole interactions are weak, a consequence of the dilution of Pd sites by tin. On the catalyst $Pd_{5.1}Sn_{3.8}$/A1, which has a larger proportion of tin (Sn/Pd atomic ratio = 2/3), absorption is restricted to the 2060–2090 cm^{-1} region; hence, no bridged species are formed either upon increasing (Fig. 3a) or decreasing CO pressure (Fig. 3b). In the latter case, no frequency shift is detected, which is the signature of *isolated end-on species*; in addition, these species are completely removed by outgassing at 373 K. In this case the CO/Pd surface stoichiometry can be considered equal to 1. When bridged species are present ($Pd_{5.0}$/A1 and $Pd_{5.2}Sn_{0.8}$/A1), the value of this ratio may approach unity if the proportion of compressed B_2 and B_2L species is higher than that of isolated B_2 entities, which is realized under about 100 Torr.

3.2. *Temperature-Programmed Reduction*

The TPR profiles of catalysts supported on A-1 are presented in Fig. 4 (see also Table 2): (i) *Below ambient*

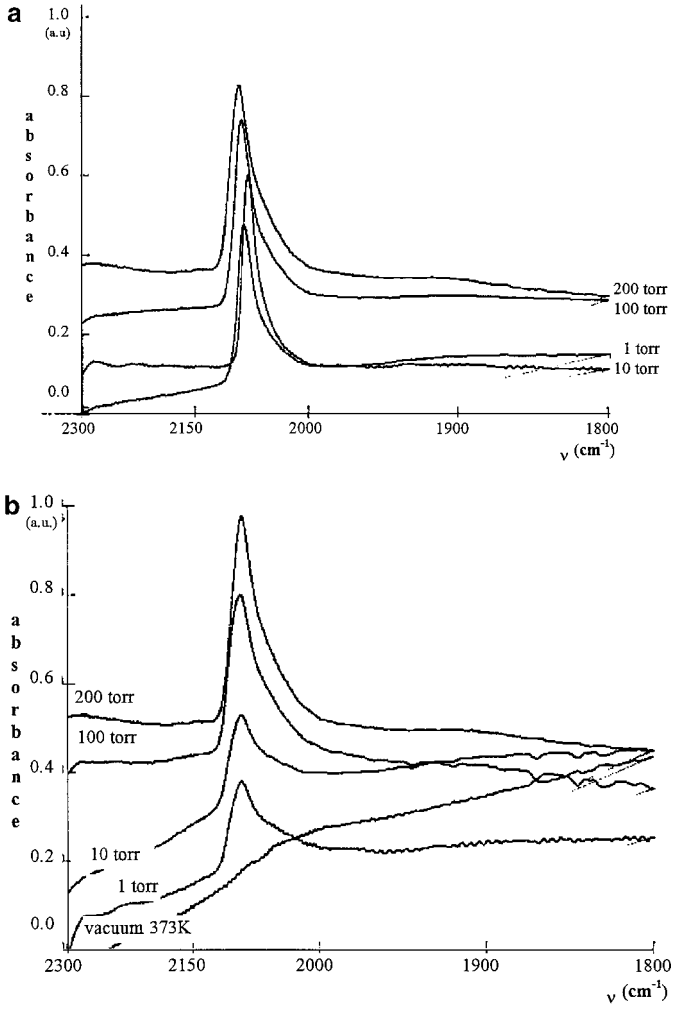

FIG. 3. Sample $Pd_{5.1}Sn_{3.8}$/A1. IR spectrum of CO adsorbed under (a) *increasing* pressure; (b) *decreasing* pressure.

temperature, the Pd ($Pd_{5.0}$/A1) and Pd–Sn ($Pd_{5.1}Sn_{3.8}$/A1, $Pd_{4.9}Sn_{5.0}Et$/A1, $Pd_{5.2}Sn_{0.8}$/A1) samples show hydrogen consumption ascribed to the reduction of Pd oxide (13, 14). Some samples ($Pd_{5.0}$/A1 and $Pd_{5.1}Sn_{3.8}$/A1) present two peaks; this may be ascribed to the presence of two oxide phases interacting differently with the support, which may generate a broad metal particle size distribution. On the other hand, the sample $Pd_{5.2}Sn_{0.8}$/A1, which shows an intense narrow peak, presents the smaller mean particle size (2.5 nm) (5). (ii) *Above ambient temperature*, samples $Pd_{5.0}$/A1 to $Pd_{5.2}Sn_{0.8}$/A1 show "negative" peaks at around 343 K, ascribed to the H_2 desorption generated by the decomposition of the β-PdH phase formed during the low-temperature reduction (15–19); they exhibit also reduction peaks at ca. 423 K, assigned to the reduction of residual Pd^{2+} ions (surrounded by remaining chloride ions) and to the reduction of Sn ions assisted by Pd atoms, with subsequent formation of Pd_xSn_y alloys.

In addition, $Pd_{5.1}Sn_{3.8}$/A1 shows also a continuous hydrogen consumption up to higher temperatures (>473 K), indicating the reduction of other tin species. This is not observed on $Pd_{4.9}Sn_{5.0}Et$/A1; this difference may be explained by a smaller amount of chloride ions in the latter sample (part 1 of this work (5) as ethanol was used as a solvent for $SnCl_2$ instead of aqueous hydrochloric acid.

The alumina properties also have an influence on the TPR profiles; in $Pd_{4.6}$/A2 (A2 support, Fig. 5), the first reduction peak is larger and starts at a higher temperature than that in the homologous catalysts supported on A1

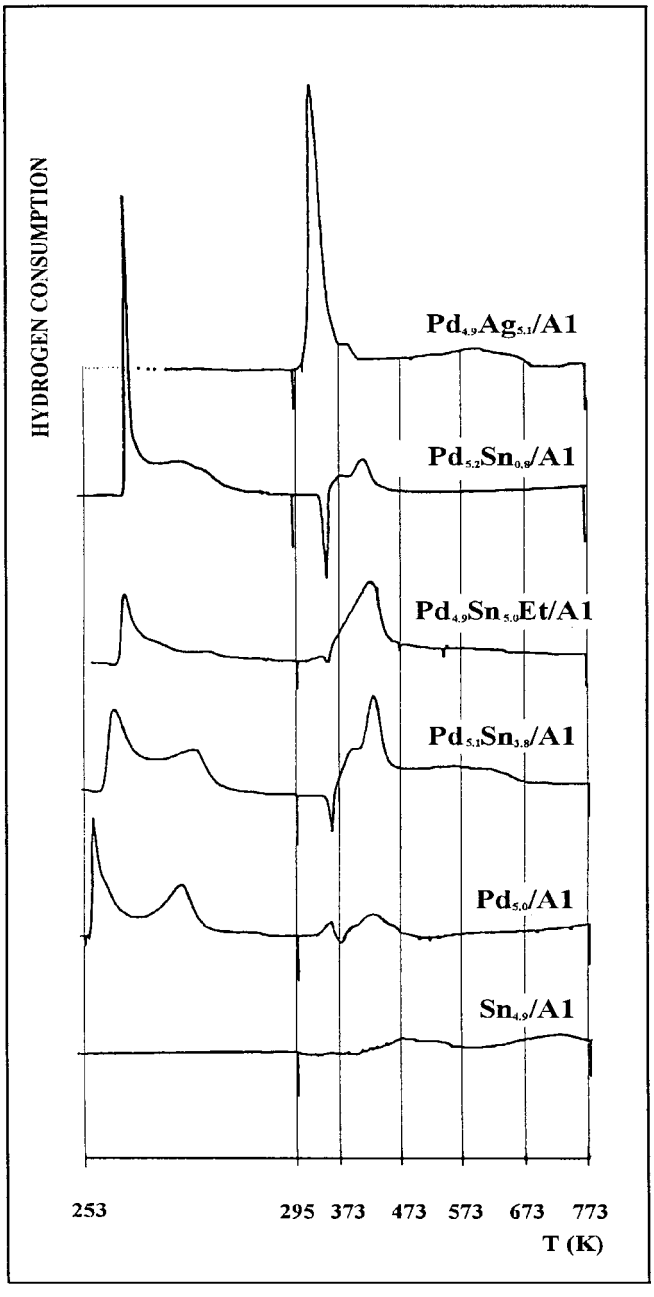

FIG. 4. TPR diagrams of samples supported on alumina A-1.

TABLE 2

Quantification of Hydrogen Consumption in TPR Analyses (μmol of H_2/g of Catalyst)

Catalyst (1)	H_2 $T <$ r.t.[a] (2)	β-PdH (3)	H_2 between r.t. and 773 K (4)	Total H_2 from TPR (5) = (2) + (4) − (3)	H_2 calculated for *total* *Pd* reduction (6)	H_2 calculated for *total* reduction[b] (7)	% of PdO reduced below r.t. (8) = [(2) − (3)]/(6)
$Pd_{5.0}$/A1	40.4	2.2	7.9	46.1	47.5	47.5	80.4
$Pd_{5.1}Sn_{3.8}$/A1	33.8	1.5	54.7	87.0	48.5	112.3	66.6
$Pd_{4.9}Sn_{5.0}$Et/A1	25.8	0.9	47.9	72.8	46.0	129.6	54.1
$Pd_{5.2}Sn_{0.8}$/A1	41.9	4.4	12.2	49.7	48.6	61.6	77.1
$Pd_{4.9}Ag_{5.1}$/A1	—	—	54.5	54.5	46.3	70.1	0
$Sn_{4.9}$/A1	—	—	10.1	10.1	—	83.1	—
$Pd_{4.6}$/A2	31.6	1.8	11.2	41.0	42.8	42.8	69.6
$Pd_{4.1}Sn_{4.5}$/A2	18.6	—	53.8	72.4	38.7	114.5	48.1
$Pd_{3.8}Ag_{5.2}$/A2	—	—	54.3	54.3	35.4	59.7	0

[a] Room temperature.
[b] Based on the total reduction of Pd(II), Ag(I), and Sn(IV) oxides, using the loading of Table 1.

($Pd_{5.0}$/A1, Fig. 4). These results are explained by a higher precursor–support interaction in the case of A-2; this carrier, more acidic than A-1, interacts more strongly with the Pd precursor $PdCl_4^{2-}$ (5), generating upon calcination, prior to TPR experiments, smaller PdO particles in strong interaction with the support, which are expected to be reduced at relatively higher temperatures.

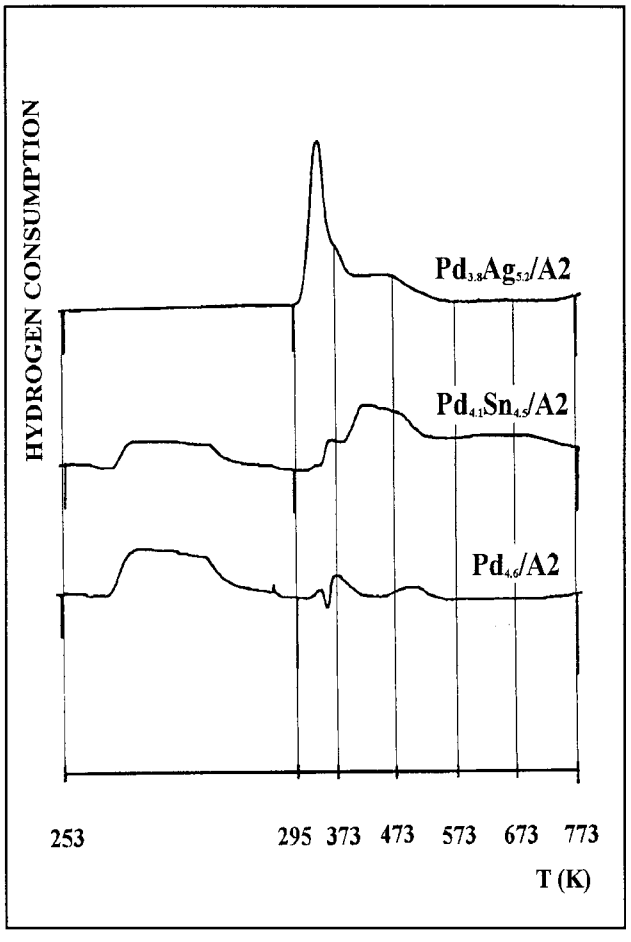

FIG. 5. TPR diagrams of samples supported on alumina A-2.

Conversely, in the case of Pd–Ag catalysts, neither $Pd_{4.9}Ag_{5.1}$/A1 (Fig. 4) nor $Pd_{3.8}Ag_{5.2}$/A2 (A-2 support, Fig. 5) exhibit subambient hydrogen consumption, which means that the presence of silver postpones the reduction of palladium. In both cases, PdO may be covered by Ag_2O in the initial samples; hence, the reduction of the former is retarded by the shell of silver oxide. This shell is then reduced first, which allows the immediate reduction of the PdO core. In this temperature range (300–400 K), the Pd hydride cannot be formed as its formation is expected at temperatures lower than ca. 300 K (16) (it is relevant to note that the negative peak related to the hydride decomposition is not observed in both cases). The final reduced Pd–Ag samples differ in particle size and homogeneity: on $Pd_{4.9}Ag_{5.1}$/A1, the Pd mean particle size is larger (29 nm) than on $Pd_{4.9}Ag_{5.1}$/A2 (5 nm) (5); moreover, a Pd–Ag alloy was identified by DRX on the latter, with a surface enrichment in silver evidenced from EDX (5) and XPS (see section 3.4) data. These results should be compared with previous data obtained on silica-supported Pd–Ag catalysts (20); in this study, solid solutions and unalloyed Ag were also evidenced; the silver-poor particles incorporate more hydrogen than the silver-rich particles and the formation of hydride was not observed for silver concentrations greater than 60%.

Moreover, concerning these Pd–Ag samples, the small hydrogen consumption observed at higher temperatures ($T > 373$ K) is ascribed to the reduction of the remaining *isolated* Ag_2O particles, and these signals are more pronounced on $Pd_{3.8}Ag_{5.2}$/A2 because this catalyst presents a higher Ag/Pd atomic ratio (1.37, see Table 1).

Table 2 shows a tentative quantification of hydrogen consumption, based on a CuO standard. In the last column

are presented the percentages of PdO reduced below r.t: it is confirmed that (i) the carrier A-2 delays the reduction of Pd catalysts (compare $Pd_{5.0}$/A1 and $Pd_{4.6}$/A2) and of Pd–Sn catalysts as well ($Pd_{5.1}Sn_{3.8}$/A1 and $Pd_{4.1}Sn_{4.5}$/A2); (ii) the presence of silver ($Pd_{4.9}Ag_{5.1}$/A1 and $Pd_{3.8}Ag_{5.2}$/A2) inhibits Pd reduction below r.t. but in these catalysts both metals are almost completely reduced up to the final temperature employed (773 K), the differences between measured and calculated amounts being ascribed to the presence of metallic Ag in calcined samples (5); (iii) $Pd_{5.1}Sn_{3.8}$/A1 shows a higher H_2 consumption than $Pd_{4.9}Sn_{5.0}$Et/A1 (ca. 77% and ca. 56% of the amount calculated for the total reduction of both metals, respectively). This should be explained by the higher Pd/Sn atomic ratio of the former (it is known that Pd catalyzes the Sn reduction).

3.3. ^{119}Sn Mössbauer Spectroscopy

Figure 6 shows the Mössbauer spectra of the tin-containing *calcined* samples and of bulk SnO_2 as a reference. The corresponding Mössbauer parameters are reported in Table 3 in addition to the chemical species identified. All catalysts exhibited two types of Sn^{IV} species, one like bulk SnO_2 and the other with higher quadrupole splitting values (less symmetric environment); the latter may be ascribed to SnO_2 interacting with alumina (21) or forming $SnAl_2O_5$ (22). However, $Pd_{5.1}Sn_{3.8}$/A1 exhibits almost no interacting Sn^{IV} species, showing that its formation is influenced by the support and the preparation procedure (compare $Pd_{5.1}Sn_{3.8}$/A1 with $Pd_{4.1}Sn_{4.5}$/A2 and $Pd_{4.9}Sn_{5.0}$Et/A1, respectively).

TABLE 3

Mössbauer Parameters and Assignments for Calcined Samples (cf. Fig. 6)

Catalyst	Isomer shift (mm/s)[a]	Quadrupole splitting (mm/s)[a]	Relative intensity (%)[b]	Assignment
$Pd_{5.1}Sn_{3.8}$/A1	−0.08	0.56	96	SnO_2
	0.16	0.89	4	$SnAl_2O_5$
$Pd_{4.9}Sn_{5.0}$Et/A1	0.00	0.53	66	SnO_2
	0.03	0.81	34	$SnAl_2O_5$
$Pd_{5.2}Sn_{0.8}$/A1	−0.04	0.53	60	SnO_2
	0.02	0.65	40	$SnAl_2O_5$
$Sn_{4.9}$/A1	−0.05	0.46	60	SnO_2
	0.16	0.89	40	$SnAl_2O_5$
$Pd_{4.1}Sn_{4.5}$/A2	0.00	0.46	66	SnO_2
	0.03	0.99	34	$SnAl_2O_5$
SnO_2	0.00	0.54	100	Standard

[a] (±0.02).
[b] (±3%).

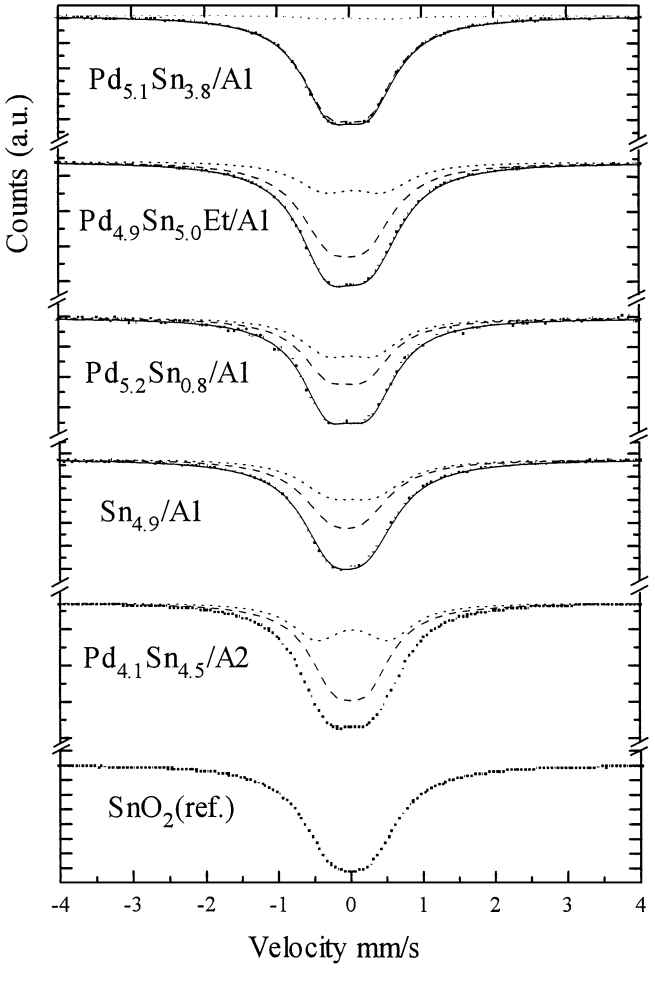

FIG. 6. Mössbauer spectra of calcined samples.

Figure 7 shows the Mössbauer spectra of *reduced* samples and the corresponding Mössbauer parameters are reported in Table 4, in addition to the chemical species identified. Estimation of the composition was based on (i) the linear correlation between the atomic tin composition in Pd–Sn compounds and the corresponding isomer shift (23) and (ii) earlier XRD results (5).

The *reduced* samples contain (i) the SnO_2 and $SnAl_2O_5$ phases already identified in the calcined samples, (ii) various bimetallic phases that represent between 36 and 67 wt% of total tin, depending on the sample considered (Table 4). As about half of the total tin amount remains as Sn^{IV}, the Sn/Pd ratio in the metallic phases is expected to be lower than the total one (Table 1). It should also be noted that the reducing treatment increases significantly the amount of Sn^{IV} species interacting with alumina in $Pd_{5.1}Sn_{3.8}$/A1.

Conversely, the SnO_2/Al_2O_3 sample ($Sn_{4.9}$/A1) proved to be almost irreducible, containing about 96% of Sn^{IV} and *traces* of Sn^{II} and of *nonidentified* species; this information is in agreement with the tentative quantification of the TPR results (Table 2).

The catalysts $Pd_{5.1}Sn_{3.8}$/A1 and $Pd_{4.1}Sn_{4.5}$/A2, prepared in the same way on aluminas A-1 and A-2, present similar

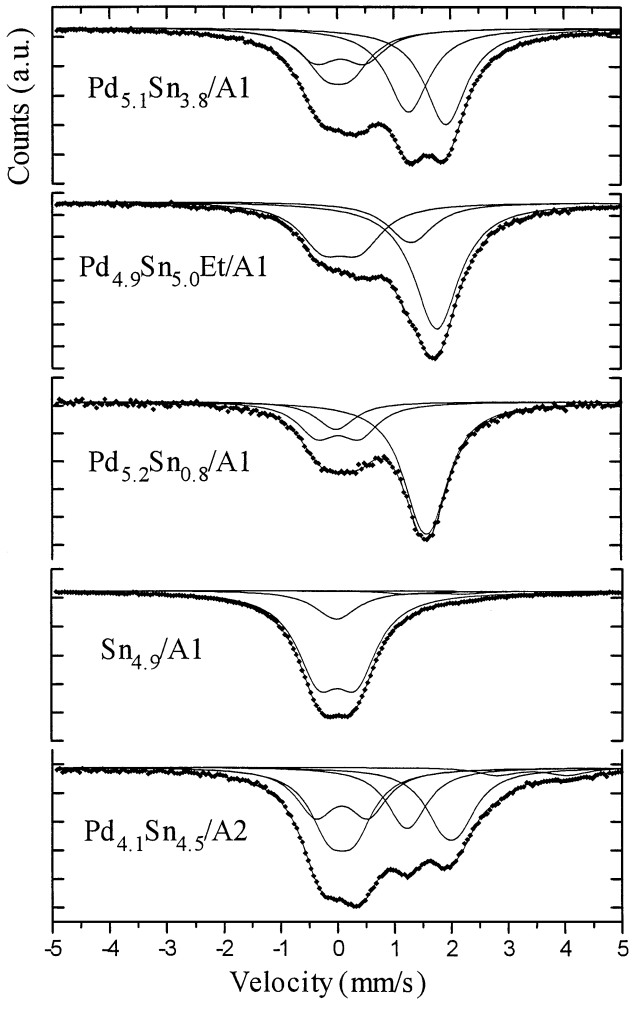

FIG. 7. Mössbauer spectra of reduced samples.

Mössbauer spectra. The Pd_2Sn compound (23) was identified by X-ray diffraction on both catalysts (5). This information, in conjunction with the Pd–Sn Mössbauer data found in the literature (24), was used as reference for the other assignments (Table 4). In accordance with this *isomer shift* parameter scale, the same two types of Sn^0 species are detected on both catalysts: one is associated with this Pd_2Sn compound (IS $\approx$ 1.93) and the other is ascribed to a *Sn-poor* PdSn solid solution (IS $\approx$ 1.25).

Both samples $Pd_{4.9}Sn_{5.0}Et/A1$ and $Pd_{5.2}Sn_{0.8}/A1$ contain a Sn-poor Pd–Sn solid solution and the Pd_3Sn intermetallic compound, although the total Sn/Pd ratio is high for the former (0.91) and low for the latter (0.13); this peculiarity of $Pd_{4.9}Sn_{5.0}Et/A1$ may arise from the nature of the solvent used for the preparation (ethanol, cf. section 3.2); a low-valence Pd–Sn complex (bimetallic Sn^{II} and Pd^{I} species) was observed upon alcoholic tin impregnation (5). Even though this complex is destroyed upon calcination, the contact between Sn and Pd should be more intimate than that upon impregnation in an aqueous hydrochloric medium. Hence, the nature of the Pd–Sn intermetallic phases formed seem to be influenced by the Sn/Pd atomic ratio, the impregnation medium, and the acidity of the support.

3.4. XPS Studies

As a large part of tin is present as SnO_2, XPS analysis could not give reliable information on the surface composition of metal particles in Pd–Sn samples; hence, experiments were focused on Pd–Ag samples (Table 5). The binding energies measured for Ag $3d_{5/2}$ are significantly lower than that of bulk silver; this result could be explained by a partial charge transfer from Ag to Pd (4), but it may also be due to varying *d–d* electron interactions among the silver atoms in the alloy (1b). A relevant result is the surface enrichment in silver (Table 5): in sample $Pd_{4.9}Ag_{5.1}/A2$, which contains Pd–Ag alloy (5), this is expected from thermodynamic considerations (1b, 4, 20) and already reported for

TABLE 4

Mössbauer Parameters[a] and Assignments for Reduced Samples (cf. Fig. 7)

Catalyst	Isomer shift (mm/s)[b]	Quadrupole splitting (mm/s)[b]	Relative intensity (%)[c]	Assignment
$Pd_{5.1}Sn_{3.8}/A1$	0.02	0.40	20	SnO_2
	0.04	0.85	22	$SnAl_2O_5$
	1.26	—	27	PdSn solution[d]
	1.92	—	31	Pd_2Sn
$Pd_{4.9}Sn_{5.0}Et/A1$	0.08	0.29	10	SnO_2
	0.08	0.82	23	$SnAl_2O_5$
	1.28	—	17	PdSn solution[d]
	1.75	—	46	Pd_3Sn
	2.26	—	3	n.i.[e]
	2.62	1.21	1	n.i.[e]
$Pd_{5.2}Sn_{0.8}/A1$	−0.06	0.37	23	SnO_2
	0.04	0.90	16	$SnAl_2O_5$
	1.48	—	39	PdSn solution[d]
	1.73	—	22	Pd_3Sn
$Sn_{4.9}/A1$	−0.01	0.47	64	SnO_2
	0.00	0.87	32	$SnAl_2O_5$
	1.25	—	1.6	n.i.[e]
	2.20	—	1.5	n.i.[e]
	3.45	1.28	0.9	$SnAl_2O_4$
$Pd_{4.1}Sn_{4.5}/A2$	0.08	0.47	35	SnO_2
	0.08	1.01	21	$SnAl_2O_5$
	1.24	—	18	PdSn solution[d]
	1.94	—	19	Pd_2Sn
	2.43	—	4	n.i.[e]
	3.49	1.18	3	$SnAl_2O_4$

[a] Quadrupole splitting = 0 (local symmetrical environment of tin atoms).
[b] (±0.02).
[c] Percentage of total tin (±3%).
[d] Sn < 16%.
[e] n.i. = not identified.

TABLE 5

XPS Binding Energies and Atomic Ratios on Pd–Ag Catalysts

Sample	Pd $3d_{5/2}$ (eV)	Ag $3d_{5/2}$ (eV)	$(Ag/Pd)_s$	$(Ag/Pd)_b$
$Pd_{4.9}Ag_{5.1}/A1$	334.3	367.1	2.5	1.04
$Pd_{3.8}Ag_{5.2}/A2$	334.7	367.4	2.7	1.38

unsupported (25, 26), silica-supported (20, 27), and pumice-supported (28) Pd–Ag catalysts; in sample $Pd_{4.9}Ag_{5.1}/A1$ (predominance of separated Pd and Ag metallic phases), it is explained by the presence of a silver shell on a palladium core. It must be recalled, however, that the data obtained here represent mean values as a part of silver is unalloyed (5).

4. CONCLUSIONS

In the Pd–Sn catalysts, the ^{119}Sn Mössbauer measurements show that, after reduction at the standard procedure (up to 773 K), tin is present as SnO_2 and $SnAl_2O_5$, along with a *Sn-poor* PdSn solid solution and Pd_xSn_y intermetallic phases. Hence, the Sn/Pd ratio in the metallic phases is expected to be lower than the total one. An intermetallic compound Pd_2Sn and a Sn-poor (<16%) PdSn solid solution were identified in the bimetallic catalysts prepared by acid impregnation, with a total Sn/Pd atomic ratio between 2/3 and 1. Another intermetallic phase, Pd_3Sn, was observed either by lowering the initial Sn/Pd atomic ratio or by introducing tin through alcoholic impregnation. Hence, the nature of the Pd–Sn intermetallic phases formed seems to be influenced mainly by the Sn/Pd atomic ratio and the impregnation medium.

These results are in agreement with the surface studies performed by IR spectroscopy of adsorbed CO: when the Sn/Pd atomic ratio increases, the intensity ratio between linear and bridged CO species increases and the dipole–dipole interactions decrease, which characterizes the dilution of Pd sites.

In opposition to tin, the presence of silver postpones the reduction of PdO in calcined catalysts; this is ascribed to the presence of an Ag_2O shell on a PdO core, which upshifts the reduction temperature of PdO in a range where the formation of β-Pd hydride is no more favored This leads to a surface enrichment in silver.

Finally, as shown in Ref. (6), the catalysts performances (activity and also selectivity) in the hydrogenation of hexa-1,3-diene and hexa-1,5-diene are correlated with the nature of the metallic phases described above.

ACKNOWLEDGMENTS

The authors are grateful to Mrs. F. Nectoux for her assistance in Mössbauer experiments and to the CNPq (Brazil) for the financial support that allowed this international cooperation.

REFERENCES

1. (a) Bond, G. C., "Catalysis by Metals," p. 297. Academic Press, London, 1962. (b) Ponec, V., and Bond, G. C., "Catalysis by Metals and Alloys." Elsevier, Amsterdam, 1995.
2. Borgna, A., Moraweck, B., Massardier, J., and Renouprez, A., *J. Catal.* **128**, 99 (1991).
3. (a) Young, W. G., Meier, R. L., Vinograd, J., Bollinger, H., Kaplan, L., and Linden, S. L., *J. Am. Chem. Soc.* **69**, 2046 (1947). (b) Fragale, C., Gargano, M., Ravasio, N., Rossi, M., and Santo, I., *J. Mol. Catal.* **24**, 211 (1984).
4. Sales, E. A., Benhamida, B., Caizergues, V., Lagier, J.-P., Fiévet, F., and Bozon-Verduraz, F., *Appl. Catal. A* **172**, 273 (1998).
5. Sales, E. A., Bugli, G., Ensuque, A., Mendes, M. J., and Bozon-Verduraz, F., *Phys. Chem. Chem. Phys.* **1**, 491 (1999).
6. Sales, E. A., Mendes, M. J., and Bozon-Verduraz, F., *J. Catal.* **195**, 96 (2000).
7. Hurst, N. W., Gentry, S. J., Jones, A., and Mc Nicol, B. D., *Catal. Rev.-Sci. Eng.* **24**, 233 (1982).
8. Sheppard, N., and Nguyen, T. T., *Adv. IR Raman Spectros.* **5**, 67 (1978).
9. Tessier, D., Rakai, A., and Bozon-Verduraz, F., *J. Chem. Soc. Faraday. Trans.* **88**, 741 (1992).
10. Della Gatta, G., Fubini, B., Ghiotti, G., and Morterra, C., *J. Catal.* **43**, 90 (1976).
11. Binet, C., Jadi, A., and Lavalley, J. C., *J. Chim. Phys.* **86**, 451 (1989).
12. Gelin, P., Siedle, A. R., and Yates, J. T., Jr., *J. Phys. Chem.* **88**, 2978 (1984).
13. Lieske, H., Lietz, G., Hanke, W., and Völter, J., *Z. Anorg. Allg. Chem.* **527**, 135 (1985).
14. Juszczyk, W., Karpinski, Z., Ratajczykowa, I., Stanasiuk, Z., Zielinski, J., Shieu, L.-L., and Sachtler, W. M. H., *J. Catal.* **120**, 68 (1989).
15. Karpinski, Z., *Adv. Catal.* **37**, 45 (1990).
16. Palczewska, W., *Adv. Catal.* **24**, 245 (1975).
17. Scholten, J. J. S., and Konvalinka, J. A., *J. Catal.* **5**, 1 (1966).
18. Lynch, J. F., and Flanagan, T. B., *J. Phys. Chem.* **77**(22), 2628 (1973).
19. Chen, G., Tsae, W., and Yeh, C. T., *Appl. Catal.* **8**, 3 (1983).
20. El Hamdaoui, A., Bergeret, G., Massardier, J., Primet, M., and Renouprez, A., *J. Catal.* **148**, 47 (1994).
21. Li, Y.-X., and Klabunde, K. J., *J. Catal.* **126**, 173 (1990).
22. (a) Gray, P. R., and Farha, F. E., *in* "Mössbauer Effect Methodology" (I. J. Gruverman and W. Seidel, Eds.), Vol. 10, p. 47. Plenum, New York, 1976. (b) Snediker, D. K., *in* "Mössbauer Effect Methodology" (I. J. Gruverman and W. Seidel, Eds.), Vol. 2, p. 161. Plenum, New York, 1966.
23. Elliot, R. P., *in* "Constitution of Binary Alloys," First Supplement, p. 732. McGraw-Hill, New York, 1986.
24. Cordey Hayes, M., and Harris, I. R., *Phys. Lett. A* **24**, 80 (1967).
25. Reniers, F., Delplancke, M. P., Asskali, A., Jardinier-Offergeld, M., and Bouillon, F., *Appl. Surf. Sci.* **81**, 151 (1994).
26. Kuijers, F. J., and Ponec, V., *J. Catal.* **60**, 100 (1979).
27. Sachtler, W. M. H., *Catal. Rev.-Sci. Eng.* **14**(2), 193 (1976).
28. Venezia, A. M., Liotta, L. F., Deganello, G., Schay, Z., and Guczi, L., *J. Catal.* **182**, 449 (1999).